MMC-Based SRM Drives with Decentralized Battery Energy Storage System for Hybrid Electric Vehicles

Chun Gan, *Member, IEEE*, Qingguo Sun, Jianhua Wu, Wubin Kong, *Member, IEEE*,

Cenwei Shi, *Member, IEEE*, and Yihua Hu, *Senior Member, IEEE*

***Abstract*—This paper proposes a modular multilevel converter (MMC)-based switched reluctance motor (SRM) drive with decentralized battery energy storage system (BESS) for hybrid electric vehicle (HEV) applications. In the proposed drive, a battery cell and a half-bridge converter is connected as a submodule (SM), and multiple SMs are connected together for the MMC. The modular full-bridge converter is employed to drive the motor. Flexible charging and discharging functions for each SM are obtained by controlling switches in SMs. Multiple working modes and functions are achieved. Compared to conventional and existing SRM drives, there are several advantages for the proposed topology. A lower dc bus voltage can be flexibly achieved by selecting SM operation states, which can dramatically reduce the voltage stress on the switches. Multilevel phase voltage is obtained to improve the torque capability. Battery state-of-charge (SOC) balance can be achieved by independently controlling each SM. Flexible fault-tolerance ability for battery cells is equipped. The battery can be flexibly charged in both running and standstill conditions. Furthermore, completely modular structure is achieved by using standard half-bridge modules, which is beneficial for market mass production. Experiments carried out on a three-phase 12/8 SRM confirm the effectiveness of the proposed SRM drive.**

***Index Terms*—Modular multilevel converter (MMC), hybrid electric vehicle (HEV), charging and discharging, flexible dc bus voltage, battery fault tolerance, switched reluctance motor (SRM).**

This manuscript has never been presented at a conference or submitted elsewhere previously.

Chun Gan is with the Department of Electrical Engineering and Computer Science, University of Tennessee, Knoxville, TN 37996, USA. (E-mail: cgan@utk.edu)
Qinguo Sun, Jianhua Wu, and Cenwei Shi are with the College of Electrical Engineering, Zhejiang University, Hangzhou, China. (E-mail: lwsunqg@163.com; hzjhwu@163.com; singing@zju.edu.cn)
Wubin Kong is with the School of Electrical and Electronic Engineering, Huazhong University of Science and Technology, Wuhan, China. (E-mail: wubinkong@126.com)
Yihua Hu is with the Department of Electrical Engineering and Electronics, University of Liverpool, Liverpool, U.K. (E-mail: y.hu35@liverpool.ac.uk)

I. INTRODUCTION

With clean energy requirements in urban transportations, electric vehicles (EVs) and hybrid EVs (HEVs) have received much attention owing to their fuel-efficient performance and protection of the environment against exhaust emission, which have been significantly supported all over the world [1]-[5]. However, considering the driving range anxiety issue and control flexibility, HEVs have been a compromise solution for EVs and traditional petrol vehicles. For HEV powertrain systems, permanent magnet motors are popular due to high torque and high efficiency. However, permanent magnets that made from rare-earth materials should be used for these motors, which are high cost and decrease the motor reliability and performance in high-temperature and high-speed operations. To overcome these shortcomings, much effort is focused on developing rare-earth-free motors for EVs/HEVs [6], [7].

SRMs are known to have a more robust structure due to no rotor windings and permanent magnets, which can provide a more low-cost topology and a longer operation time in high-temperature environments. Also, they have a much wider speed range compared to other motors, which is very important for electric powertrains. Because of further advantages, such as high torque, simple structure, high reliability, and excellent fault-tolerance ability, SRMs have become a promising solution for powertrain systems [8]-[15].

Some improved SRM converter topologies have been proposed for system performance improvements. In [16]-[19], three-phase full-bridge converters are used for SRM drives to achieve modular topology. An asymmetric three-level neutral-point diode-clamped converter is proposed in [20] to reduce the torque ripple and improve the system efficiency. A dual supply buck-boost converter is introduced for SRM drives in [21] to provide soft starting, reduce the torque ripple, and improve the power density. In [22], a quasi-Z-source integrated converter is presented, which can reduce the dc-link capacitance and extend the speed range. In [23]-[25], multilevel converters are developed to improve the phase voltage in the winding excitation and demagnetization regions to reduce the current rising and falling times for high-speed operations.

For EVs/HEVs, the wide operational speed, torque demand, and integrated converter functions in vehicular applications pose challenges to the traction system design. A motor drive system can be used for driving a traction motor as well as for charging the battery. The overall efficiency of the electrified traction drive can be improved due to the single conversion stage between the battery and motor. Therefore, SRM drives with integrated charging functions have been developed in [26]-[30] for EV/HEV applications.

A split converter for four-phase SRMs is proposed in [26] for EVs, and a central-tapped winding node is introduced to connect the phase windings and converter circuit, where on-board charging is achieved. However, traditional phase winding structure needs to be changed and it cannot be used for three-phase motors. In [27], an improved C-dump converter is presented with integrated charging capability. However, the converter topology has poor fault-tolerance ability due to reduced switches and the multilevel

phase voltage is not achieved. In [28], a tri-port drive is put forward to achieve integrated grid-connected charging ability. But the dc bus voltage cannot be flexibly changed and three phases share one switch leading to poor fault-tolerance ability. Multiport converter topologies are proposed in [29], [30] for HEVs to improve the torque performance and achieve battery charging. However, modular structure, flexible dc bus voltage, and battery fault tolerance are not achieved. In [31], modular power modules are employed to form a modified Miller converter, while fault tolerance ability for each phase and batteries are not achieved.

Considering that the required dc bus voltage in low-speed operations is much lower than that in high-speed operations, the voltage stress on the switches and the switching loss can be reduced in the inverter/converter with a lower dc bus voltage [32]. Furthermore, the reliability of the switches can be enhanced due to a much lower voltage stress [33]. Considering this point, an SRM converter with a dc-link chopper is proposed in [34], where the dc bus voltage is controlled by the chopper as a function of the motor speed. However, an additional inductor and capacitor need to be used and multilevel phase voltage is not achieved. Also, this converter is derived from a split dc-link four-switch converter without phase isolation, leading to poor fault-tolerance ability and control flexibility. SRM drives with a front-end dc-dc converter are presented in [35], [36] to obtain variable dc bus voltage and battery charging ability, while the additional use of inductors and capacitors reduces the power density, and the modular structure and flexible battery fault-tolerance ability are not achieved.

Due to the highly modular structure, multilevel voltage, and inherently bi-directional characteristic, modular multilevel converters (MMCs) have been employed for AC machines to improve sinusoidal waveforms for system performance enhancements [37]-[40]. Multilevel converter topologies have been investigated for SRMs to enhance the torque capability, improve the high-speed performance, and reduce the power loss [20], [41]. Considering that the MMC can provide not only the multilevel voltage, but also the modular structure, flexible output voltage, and independent submodule control, it can be explored for SRM drives to improve the whole system performance and achieve integrated multiple functions. For SRMs, MMCs have not been reported yet. Therefore, this paper takes the advantages of the MMC topology for SRM drives to achieve multilevel phase voltage, flexible dc bus voltage, modular structure, and flexible submodule control. By developing the MMC topology for SRM drives, the torque can be improved due to the multilevel voltage, the voltage stress on the switches can be reduced with flexible dc bus voltage. Furthermore, the flexible battery fault-tolerance ability, and flexible discharging and charging functions can be achieved due to the independent submodule control.

In the proposed MMC-based SRM drive, multiple working modes are achieved, including the battery driving mode, generator control unit (GCU) driving mode, GCU-battery driving mode, running charging mode, standstill charging mode, and battery fault-tolerance mode. The advantages of the proposed topology are: 1) multiple working modes can be flexibly selected by controlling the MMC and full-bridge converter; 2) the MMC-based topology can drive the SRM from variable dc voltages according to the running speed to reduce the voltage stress on the switches which also improves the reliability; 3) multilevel phase voltage is

achieved due to additional battery charging in running conditions, which improves the torque capability; 4) by using standard half-bridge modules for both the MMC and full-bridge converter, completely modular topology is achieved; 5) flexible charging functions can be directly achieved through the proposed drive without external ones, including the running charging and standstill charging modes; 6) flexible fault-tolerance ability for each battery cell is equipped by easily bypassing the faulty one; 7) the battery state-of-charge (SOC) can be balanced by controlling the SM charging according to the SOC level.

This paper is organized as follows. Section II presents the conventional SRM drive. Section III proposes a new MMC-based SRM drive for HEV applications; the driving mode, charging mode, variable dc bus voltage, and battery fault-tolerance mode are investigated; the current flow and phase voltage are analyzed; a detailed comparison of the proposed and existing topologies is presented. The proposed drive topology is verified by experiments in Section IV. Finally, the conclusion is given in Section V.

II. Conventional SRM Drives

Fig. 1 illustrates the diagram of a three-phase 12/8 SRM drive, mainly including a power converter, an SRM, a drive circuit, current sensors, a position sensor, and a current controller. Phase currents are detected by individual current sensors for the implementation of the current control strategy. Considering the phase isolation characteristic and excellent fault-tolerance capability, the asymmetrical half-bridge converter is usually employed for the SRM drive, where each phase leg can be independently controlled by two switching devices. For the current controller, hysteresis control method is usually used. The hysteresis control system is a nonlinear system, which has excellent loop performance, global stability, and small phase lag. Therefore, the current hysteresis control is inherently stable and robust to dynamic perturbations, and the system is more stable and has fast dynamic response due to its inherent non-linearity.

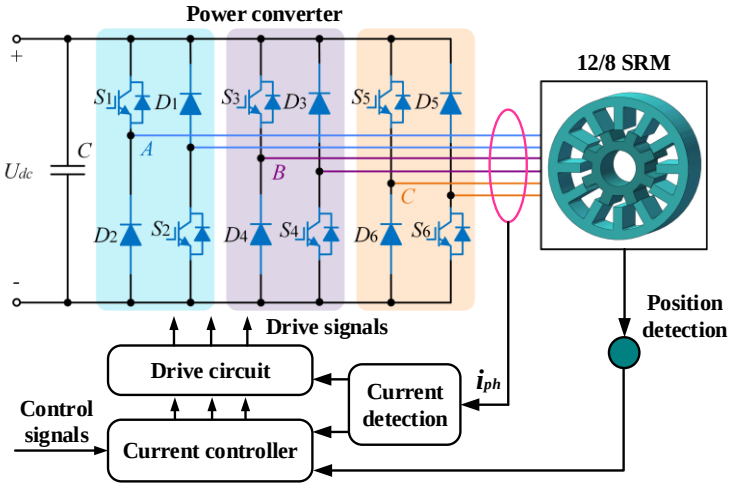

Fig. 1. Diagram of the three-phase 12/8 SRM drive.

Fig. 2 shows the three switching modes of phase A in the asymmetrical half-bridge converter, including the excitation mode, freewheeling mode, and demagnetization mode. When switches S_1 and S_2 are both turned on, the dc power source supplies the current to the phase A winding, and this phase works in the excitation mode (see Fig. 2(a)), where the phase voltage is positive dc bus voltage U_{dc}; when the switch S_1 is turned off and S_2 is still on, the phase A current flows through S_2 and diode D_2 in a zero-voltage loop (ZVL), where phase A is in the ZVL mode (see Fig. 2(b)); when switches S_1 and S_2 are both turned off, the phase A current flows back to the dc source through diodes D_1 and D_2, and phase A is in the demagnetization mode (see Fig. 2(c)), where the phase voltage is negative dc bus voltage $-U_{dc}$.

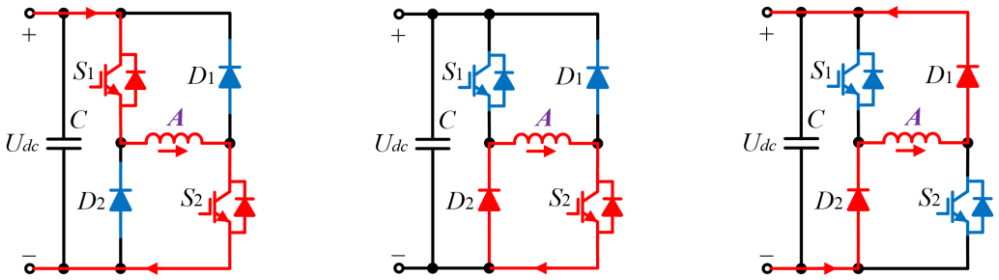

Fig. 2. Switching modes of the asymmetrical half-bridge converter. (a) Excitation mode. (b) ZVL mode. (c) Demagnetization mode.

The voltage equation for each phase can be expressed in terms of the current, inductance, and rotor position as

$$U_k = R_k i_k + L_k(\theta, i_k)\frac{di_k}{dt} + \frac{\partial L_k(\theta, i_k)}{\partial \theta}\omega i_k \tag{1}$$

where U_k is the phase voltage, R_k is the phase winding resistance, i_k is the phase current, θ is the rotor position, L_k is the phase winding inductance which varies as a function of the rotor position, ω is the rotor angular speed, and k=a, b, c phase.

The output torque of the three-phase SRM is the sum of individual phase torques, which is expressed as

$$T_e = \sum_{k=1}^{3} T_{ek} = \sum_{k=1}^{3} \frac{1}{2} i_k^{\,2} \frac{\partial L_k(i_k, \theta)}{d\theta} \tag{2}$$

When a current is applied in the inductance ascending region, a positive phase torque can be obtained; while applying a current to a phase winding in the inductance descending region leads to a negative phase torque.

The mechanical equation of the SRM is expressed as

$$J\frac{d\omega}{dt} + \mu\omega = T_e - T_l \tag{3}$$

where T_e is the output torque, T_l is the load torque, J is the combined moment of inertia of the motor and load, and μ is the combined friction coefficient of the motor and load.

However, for conventional SRM drives, the dc bus voltage is fixed and the voltage stress on switches cannot be reduced by changing the dc bus voltage according to the running speed. The multilevel phase voltage cannot be achieved which limits the output torque in high-speed operations. Also, the fault tolerance for battery cells and flexible charging functions are not achieved. This paper proposes a MMC-based SRM drive with decentralized battery energy storage system (BESS) for HEVs. Compared to conventional and existing SRM drives, the presented topology has several advantages, including flexible dc bus voltage, multilevel phase voltage, modular structure, fault-tolerance ability for battery cells, flexible running charging, grid-connecting charging, and SOC balancing capability, which will be analyzed in detail in followings.

III. Proposed MMC-Based SRM Drive with Decentralized BESS

A. Proposed MMC-Based SRM Drive

Fig. 3 shows the developed MMC with decentralized BESS. A half-bridge converter and a battery pack E_x are employed as a submodule (SM), and each SM is made up of two insulated-gate bipolar transistors (IGBTs), including a upper switch S_{x1} and a lower switch S_{x2}. The output voltage of each SM is U_{sm}, which is determined by the SM working state according to the on-off state of two switches, and multiple SMs are connected in series to form a decentralized BESS for the total dc bus voltage U_{dc}. In this configuration, battery cells are decentralized by individual SMs, and each battery cell SM can be controlled independently.

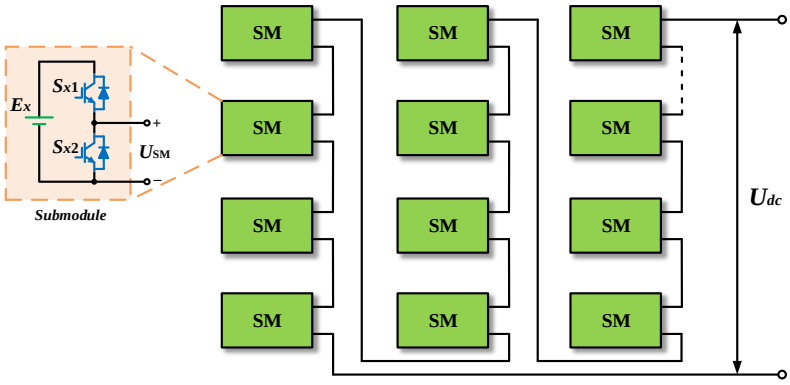

Fig. 3. Developed MMC with decentralized BESS.

As shown in Fig. 4, each SM is a two-level half-bridge converter consisting of a battery cell and two switches. In the IGBT, there is an integrated antiparallel diode. The state of the antiparallel diode is defined as on when there is a current flowing through it, and defined as off with no current. The operation states of the two-level SM under different IGBT switching states are presented in Fig. 4 and Table I.

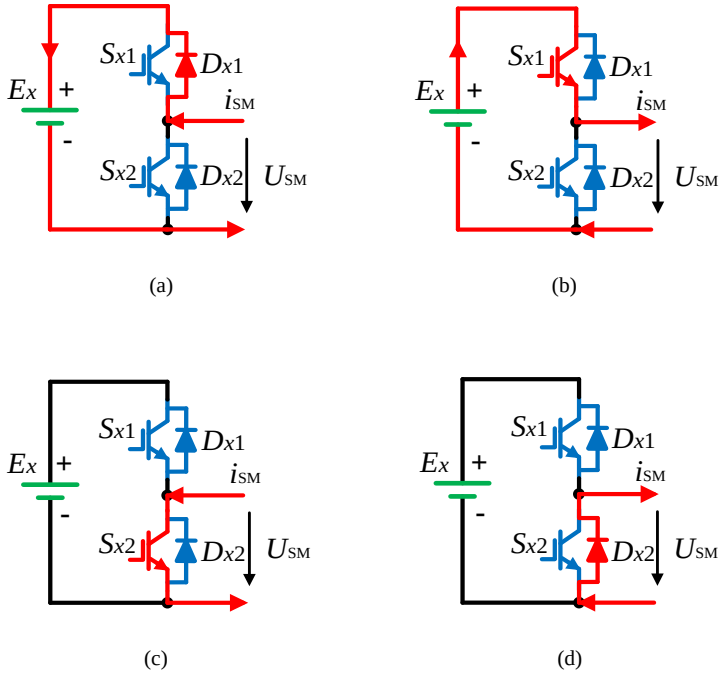

Fig. 4. Operation states of a two-level SM. (a) Discharging mode. (b) Charging mode. (c) Bypass mode 1. (d) Bypass mode 2.

TABLE I

SM OPERATION STATES

SM state	S_{x1}	S_{x2}	D_{x1}	D_{x2}	U_{sm}	i_{sm}	E_x
On	On	Off	Off	Off	U_{by}	Positive	Discharging mode
On	Off	Off	On	Off	$-U_{by}$	Negative	Charging mode
Off	Off	On	Off	Off	0	Negative	Bypass mode 1
Off	Off	Off	Off	On	0	Positive	Bypass mode 2

According to the SM working states, the switching function of SMs can be expressed by

$$U_{sm}=\begin{cases} U_{by}, & S_{x1}\ is\ on,\ S_{x2}\ is\ off,\ D_{x1}\ is\ off,\ D_{x2}\ is\ off \\ -U_{by}, & S_{x1}\ is\ off,\ S_{x2}\ is\ off,\ D_{x1}\ is\ on,\ D_{x2}\ is\ off \\ 0, & S_{x1}\ is\ off,\ S_{x2}\ is\ on,\ D_{x1}\ is\ off,\ D_{x2}\ is\ off \\ 0, & S_{x1}\ is\ off,\ S_{x2}\ is\ off,\ D_{x1}\ is\ off,\ D_{x2}\ is\ on \end{cases} \tag{4}$$

The dc bus voltage is the sum of the SM output voltages, given by

$$U_{dc}=NU_{sm} \tag{5}$$

where N is number of total SMs.

In order to illustrate the functions of the proposed drive more clearly, a simplified system with six SMs is adopted as an example in this paper for analysis. Fig. 5 shows a MMC-based SRM drive with six SMs for HEV applications, including a MMC-based decentralized BESS and a modular full-bridge converter. The full-bridge converter is used to achieve a completely modular converter structure, where the commercial power switch modules can be directly used for the proposed drive, which is beneficial for the market mass production [42]-[44]. Furthermore, the full-bridge converter can also provide a flexible fault-

tolerant operation for power switch faults with bipolar excitation [42], [43], which is suitable for high-performance and safety-critical vehicle applications. The MMC is composed of six SMs by using IGBTs with integrated fast recovery antiparallel diode, an energy storage unit including five battery packs (E_1~E_5), and a GCU including a generator (*G*), a relay (*J*), a rectifier (*RE*), and a capacitor (*C*). In the modular full-bridge converter, six half-bridge modules are used to drive the three-phase SRM, where two half-bridge modules are employed for one phase, which achieves a completely modular structure for massive production. By employing the proposed SRM drive, multiple working modes can be flexibly achieved and the system performance can be improved.

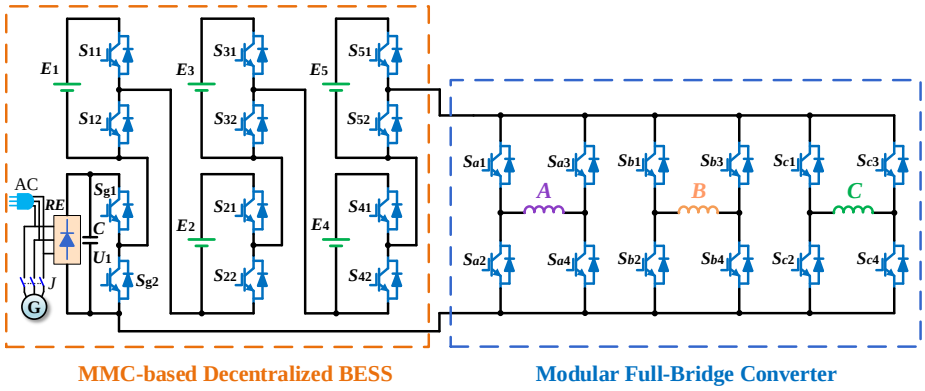

Fig. 5. MMC-based SRM drive with six SMs for HEVs.

A battery energy storage system for EVs is composed of several battery packs connected in series to satisfy a voltage and capacity specification [45], [46]. Therefore, each battery pack can be easily connected with a converter for independent control [47], [48]. For MMC topologies, the battery packs can be connected with MMC submodules for conventional AC motor drives in EVs [39], [49], [50], allowing high flexibility for the discharge and charge of each battery pack. In these papers, to reduce the complexity of the converter circuit, four to six submodules are usually adopted for phase for the proof of concept. Therefore, in this paper, in order to explain the principle of the proposed SRM drive more clearly with reduced complexity, six submodules connecting with five battery packs and a GCU are just adopted for the dc link for analysis and experiments. However, MMCs show excellent expansibility [39], [49], [50]. Hence, more flexible dc bus voltage, multilevel voltage, battery discharging and charging, and battery fault tolerance ability can be further achieved by employing more battery submodules for the proposed SRM system.

B. Battery Driving Mode

1) Full Battery Cells Driving

When the relay J is off and switch S_{g2} is on, the GCU SM is bypassed and the proposed SRM drive can work in pure-battery driving mode. In this condition, the dc bus voltage can be flexibly controlled by employing different SMs. Fig. 6 presents the working stages of the motor drive in battery control mode with flexible excitation and demagnetization voltages.

Fig. 6(a) shows the condition that E_1~ E_5 are all employed for excitation, where switches S_{11}, S_{21}, S_{31}, S_{41}, and S_{51} are all turned on, and S_{12}, S_{22}, S_{32}, S_{42}, and S_{52} are all kept off for the phase winding excitation; in the winding demagnetization mode, the current flows back to the power source through S_{11}, S_{21}, S_{31}, S_{41}, and S_{51}, as shown in Fig. 6(b). For this condition, the discharging and charging voltage for the dc link is given by

$$U_{dc} = \begin{cases} 5U_{sm}, & Discharging\ state \\ 5U_{sm}, & Charging\ state \end{cases} \tag{6}$$

The phase A voltage is directly the dc bus voltage in this condition, which can be expressed as

$$U_a = \begin{cases} 5U_{sm}, & Phase\ A\ excitation \\ -5U_{sm}, & Phase\ A\ demagnetization \end{cases} \tag{7}$$

2) Two Battery Cells Driving with Two Additional Battery Cells Charging

Fig. 6(c) and (d) present the conditions that two battery cells are employed for the winding excitation, and additional two SMs are employed to improve the voltage for winding demagnetization and achieve battery charging during running conditions. For example, E_1 and E_2 are used to supply the power to the motor, and E_3 and E_4 are employed to increase the demagnetization voltage, where S_{11} and S_{21} are both turned on, and S_{52} are also turned on to bypass the E_5 SM. In the excitation mode of phase A, the current flows through S_{11} and S_{21}, the diodes in S_{32} and S_{42}, and the bypass switch S_{52} to phase A converter, as shown in Fig. 6(c); when phase A is turned off, the demagnetization current goes through the bypass switch S_{52}, the diodes in S_{31} and S_{41}, and switches S_{11} and S_{21} to the power source, as shown in Fig. 6(d). The demagnetization voltage is elevated by E_3 and E_4, where the multilevel phase voltage can be achieved to accelerate both the excitation and demagnetization processes for torque improvements, and also E_3 and E_4 can be charged by the demagnetization current. In this condition, the charging and discharging voltage for the dc link is given by

$$U_{dc} = \begin{cases} 2U_{sm}, & Discharging\ state \\ 4U_{sm}, & Charging\ state \end{cases} \tag{8}$$

The phase A demagnetization voltage is directly increased to $-4U_{sm}$ due to additional battery cells charging. Although the dc bus voltage is only $2U_{sm}$ in the discharging mode, the excitation voltage of phase A can still be elevated to $4U_{sm}$ by phase C demagnetization, according to the current overlapping states [24], [29]. When phase C current is larger than phase A current in the

phase C demagnetization stage, phase C winding works as a current source to supply the current to phase A and simultaneously charge the battery. Because the phase C winding is under the demagnetization voltage -4U_{sm} due to the battery cell E_3 and E_4 charging, the phase A voltage can be elevated to 4U_{sm} when phase C winding supplies the current to phase A. When phase C current decreases to be smaller than phase A current, the dc-link power source and phase C both supply the current to phase A, and the phase A voltage returns to 2U_{sm}. Hence, after the excitation current quickly established at the beginning of the turn-on region with an increased voltage, the phase voltage can immediately decrease to the power supply voltage in the main turn-on region, which not only improves the torque, but also achieves a lower excitation voltage.

Therefore, multilevel phase voltage is achieved in the proposed drive and the phase A voltage can be expressed as

$$U_a = \begin{cases} 4U_{sm}, & \textit{Phase A excitation, Phase C demagnetization, } i_c > i_a \\ 2U_{sm}, & \textit{Phase A excitation, Phase C demagnetization, } i_c < i_a \\ -4U_{sm}, & \textit{Phase A demagnetization, Phase B excitation, } i_a > i_b \\ -2U_{sm}, & \textit{Phase A demagnetization, Phase B excitation, } i_a < i_b \\ -4U_{sm}, & \textit{Phase A demagnetization, Phase B in ZVL, } i_a < i_b \end{cases} \tag{9}$$

3) One Battery Cell Driving with Two Additional Battery Cells Charging

Fig. 6(e) and (f) illustrate that only E_1 is employed to supply the power, and E_2 and E_5 are used for charging, where S_{11} is turned on, and S_{32} and S_{42} are also turned on to bypass E_3 and E_4. When phase A is in the turn-on region, E_1 provides the current flowing through the switch S_{11}, the diodes of S_{22} and S_{52}, and switches S_{32} and S_{42}, as shown in Fig. 6(e); when phase A is turned off, the current goes back to the power supply through S_{42} and S_{32}, the diodes of S_{51} and S_{21}, and the switch S_{11}, as shown in Fig, 6(f). In this condition, E_2 and E_5 are employed to additionally increase the demagnetization voltage, which are also charged by the demagnetization current. The discharging and charging voltage for the dc link in this condition is given by

$$U_{dc} = \begin{cases} U_{sm}, & \textit{Discharging state} \\ 3U_{sm}, & \textit{Charging state} \end{cases} \tag{10}$$

Similarly, the phase A voltage can be expressed as follow

$$U_a = \begin{cases} 3U_{sm}, & \textit{Phase A excitation, Phase C demagnetization, } i_c > i_a \\ U_{sm}, & \textit{Phase A excitation, Phase C demagnetization, } i_c < i_a \\ -3U_{sm}, & \textit{Phase A demagnetization, Phase B excitation, } i_a > i_b \\ -U_{sm}, & \textit{Phase A demagnetization, Phase B excitation, } i_a < i_b \\ -3U_{sm}, & \textit{Phase A demagnetization, Phase B in ZVL, } i_a < i_b \end{cases} \tag{11}$$

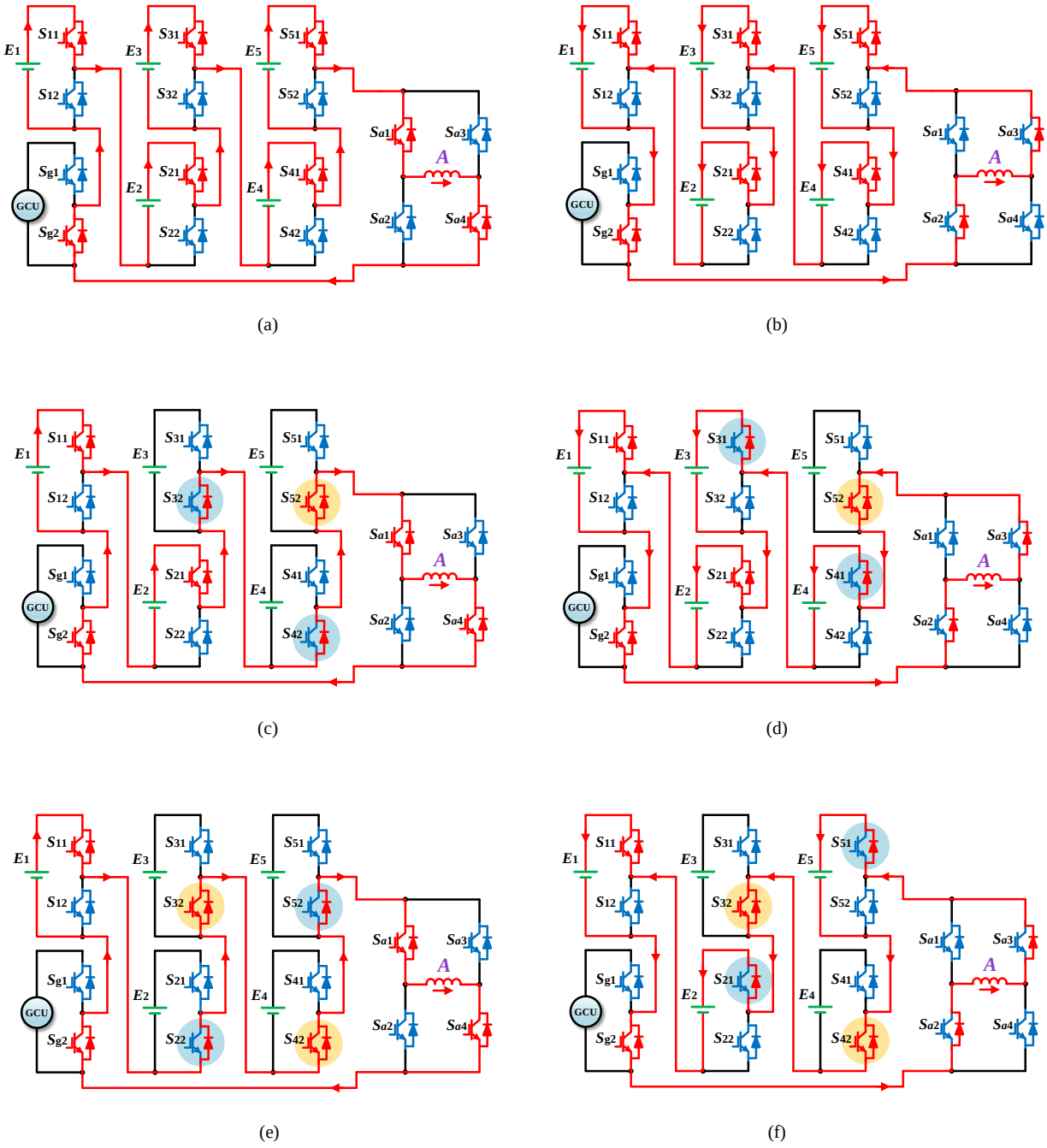

Fig. 6. Battery control mode by employing different SMs. (a) E_1~E_5 are all employed for excitation. (b) E_1~ E_5 are all employed for demagnetization. (c) E_1 and E_2 are employed for excitation. (d) E_1, E_2, E_3, and E_4 are employed for demagnetization. (e) E_1 is employed for excitation. (f) E_1, E_2, and E_5 are employed for demagnetization.

Therefore, in pure-battery driving mode, by controlling the switches in SMs, the battery cells can be flexibly selected for both excitation and demagnetization, and the dc bus voltage can be flexibly controlled according to low-speed and high-speed operations. In the phase turn-on region, k_1 SMs can be put into used for excitation, as shown in Fig. 7(a); while additional k_2 SMs can be used to increase the demagnetization voltage and achieve battery charging in the phase turn-off region, as shown in Fig. 7(b). For idle battery cells, the lower switches in corresponding SMs are turned on to make the SMs work in bypass mode; for the battery cells

that used to enhance the demagnetization voltage for the torque improvement, the demagnetization current can flow through upper switches in SMs to achieve battery charging. Battery SOC can be balanced by employing the higher-SOC battery cell for discharging and the lower-SOC battery cell for charging. The discharging and charging voltage for the dc link can be expressed as

$$U_{dc}=\begin{cases}k_1U_{sm}, & Discharging\ state\\ (k_1+k_2)U_{sm}, & Charging\ state\end{cases} \tag{12}$$

Taking phase A for example, the phase A demagnetization voltage is directly increased due to additional battery cell charging. The phase A excitation voltage can also be elevated by the phase C demagnetization, according to the current overlapping state. The phase A voltage in battery driving mode is given by

$$U_a=\begin{cases}(k_1+k_2)U_{sm}, & Phase\ A\ excitation,\ Phase\ C\ demagnetization,\ i_c>i_a\\ k_1U_{sm}, & Phase\ A\ excitation,\ Phase\ C\ demagnetization,\ i_c<i_a\\ -(k_1+k_2)U_{sm}, & Phase\ A\ demagnetization,\ Phase\ B\ excitation,\ i_a>i_b\\ -k_1U_{sm}, & Phase\ A\ demagnetization,\ Phase\ B\ excitation,\ i_a<i_b\\ -(k_1+k_2)U_{sm}, & Phase\ A\ demagnetization,\ Phase\ B\ in\ ZVL,\ i_a<i_b\end{cases} \tag{13}$$

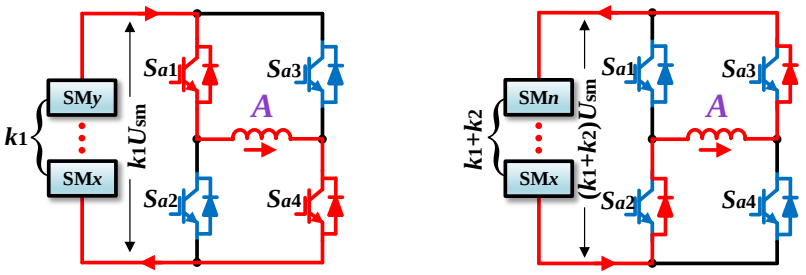

(a) (b)

Fig. 7. Battery control mode with flexible multilevel voltage and battery charging. (a) Excitation. (b) Demagnetization and battery charging.

C. GCU Driving Mode

When the relay *J* is on and switch S_{g2} is off, the GCU SM is put into use and the proposed SRM drive can work in GCU driving mode. In this mode, only GCU is used for excitation, while the multilevel phase voltage can also be achieved, and the demagnetization voltage can be increased and flexibly controlled by employing different SMs. Fig. 8 presents the working stages of the drive in GCU control mode with flexible demagnetization voltages. In the phase turn-on region, the single GCU provides the power for the phase winding excitation, as shown in Fig. 8(a); while additional k_2 SMs can be employed to increase the demagnetization voltage and achieve battery charging in the phase turn-off region, as shown in Fig. 8(b). Also, in the demagnetization mode, the lower-SOC battery cell can be employed for charging to balance the battery SOC. The charging and

discharging voltage for the dc link in GCU driving mode can be expressed in terms of the GCU output voltage and SM output voltage as

$$U_{dc}=\begin{cases}U_g, & Discharging\ state\\ -U_g-k_2U_{sm}, & Charging\ state\end{cases} \tag{14}$$

Similarly, the phase A voltage in GCU driving mode can be expressed as follow

$$U_a=\begin{cases}U_g+k_2U_{sm}, & Phase\ A\ excitation,\ Phase\ C\ demagnetization,\ i_c>i_a\\ U_g, & Phase\ A\ excitation,\ Phase\ C\ demagnetization,\ i_c<i_a\\ -U_g-k_2U_{sm}, & Phase\ A\ demagnetization,\ Phase\ B\ excitation,\ i_a>i_b\\ -U_g, & Phase\ A\ demagnetization,\ Phase\ B\ excitation,\ i_a<i_b\\ -U_g-k_2U_{sm}, & Phase\ A\ demagnetization,\ Phase\ B\ in\ ZVL,\ i_a<i_b\end{cases} \tag{15}$$

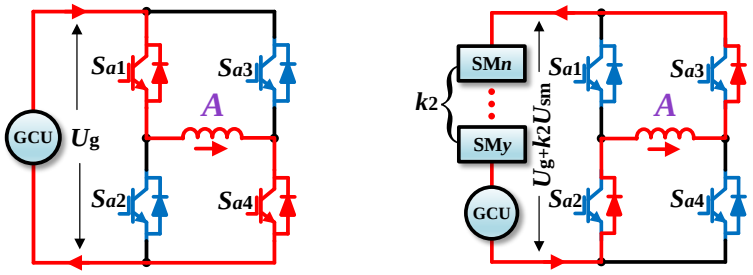

(a) (b)

Fig. 8. Battery control mode with flexible multilevel voltage and battery charging. (a) Excitation. (b) Demagnetization and battery charging.

D. GCU-Battery Driving Mode

When the relay *J* is on and switch S_{g2} is off, the GCU is put into use, and simultaneously, the battery SMs can also be employed to assist the GCU to work in GCU-battery driving mode. In this situation, the GCU and battery cells are used as a hybrid power source for both excitation and demagnetization. The multilevel phase voltage can be achieved by charging the idle SMs and the demagnetization voltage is increased to improve the torque, which is similar to the battery driving mode, where the only difference is that the GCU is used. In the winding excitation mode, the GCU and k_1 battery SMs work together to supply the power to the motor, as shown in Fig.9(a); in the winding demagnetization mode, additional k_2 battery SMs can be employed for charging, as shown in Fig.9(b), which elevate the demagnetization voltage. The charging battery cells can be flexibly selected according to the battery SOC. The charging and discharging voltage for the dc link in hybrid-source mode can be expressed as

$$U_{dc}=\begin{cases}U_g+k_1U_{sm}, & Discharging\ state\\ U_g+(k_1+k_2)U_{sm}, & Charging\ state\end{cases} \tag{16}$$

Similarly, the phase A voltage in hybrid-source mode can be expressed as follow

$$U_a = \begin{cases} U_g + (k_1 + k_2)U_{sm}, & \text{Phase A excitation, Phase C demagnetization, } i_c > i_a \\ U_g + k_1 U_{sm}, & \text{Phase A excitation, Phase C demagnetization, } i_c < i_a \\ -U_g - (k_1 + k_2)U_{sm}, & \text{Phase A demagnetization, Phase B excitation, } i_a > i_b \\ -U_g - k_1 U_{sm}, & \text{Phase A demagnetization, Phase B excitation, } i_a < i_b \\ -U_g - (k_1 + k_2)U_{sm}, & \text{Phase A demagnetization, Phase B in ZVL, } i_a < i_b \end{cases} \quad (17)$$

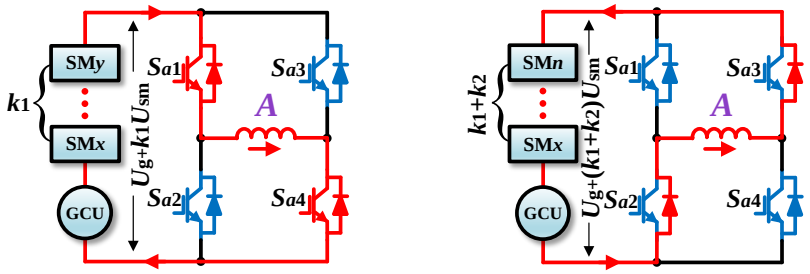

(a) (b)

Fig. 9. GCU-battery control mode with flexible multilevel voltage and battery charging. (a) Excitation. (b) Demagnetization and battery charging.

E. Standstill Charging Mode

In standstill conditions, the battery cells can be flexibly charged from the GCU or grids. There are two steps to achieve the battery charging. Firstly, the switches of phases A, B, and C are all turned on simultaneously for the winding excitation; secondly, these switches are all turned off simultaneously to make the phase currents flow back to the dc source. Fig. 10(a) shows the condition that the windings are excited by the rectification from GCU/grids, where S_{g1} is turned on. When switches S_{a1} and S_{a4}, S_{b1} and S_{b4}, S_{c1} and S_{c4} are all turned on, the current goes from the capacitor C through the switch S_{g1} and the diodes of S_{12}, S_{22}, S_{32}, S_{42}, and S_{52} to the full-bridge converter, and the energy is stored in the three phase windings. Then, switches S_{a1} and S_{a4}, S_{b1} and S_{b4}, and S_{c1} and S_{c4} are all turned off, and the current goes from phase windings through the diodes of S_{11}, S_{21}, S_{31}, S_{41}, S_{51} and the switch S_{g2} to the battery cells E_1~E_5, where full battery cell charging is achieved, as shown in Fig. 10(b). However, each battery cell can be flexibly selected for charging according to the battery SOC. For example, S_{42} and S_{52} can be turned on to bypass E_4 and E_5 during charging process, where only E_1, E_2, and E_3 are employed for charging, as shown in Fig. 10(c).

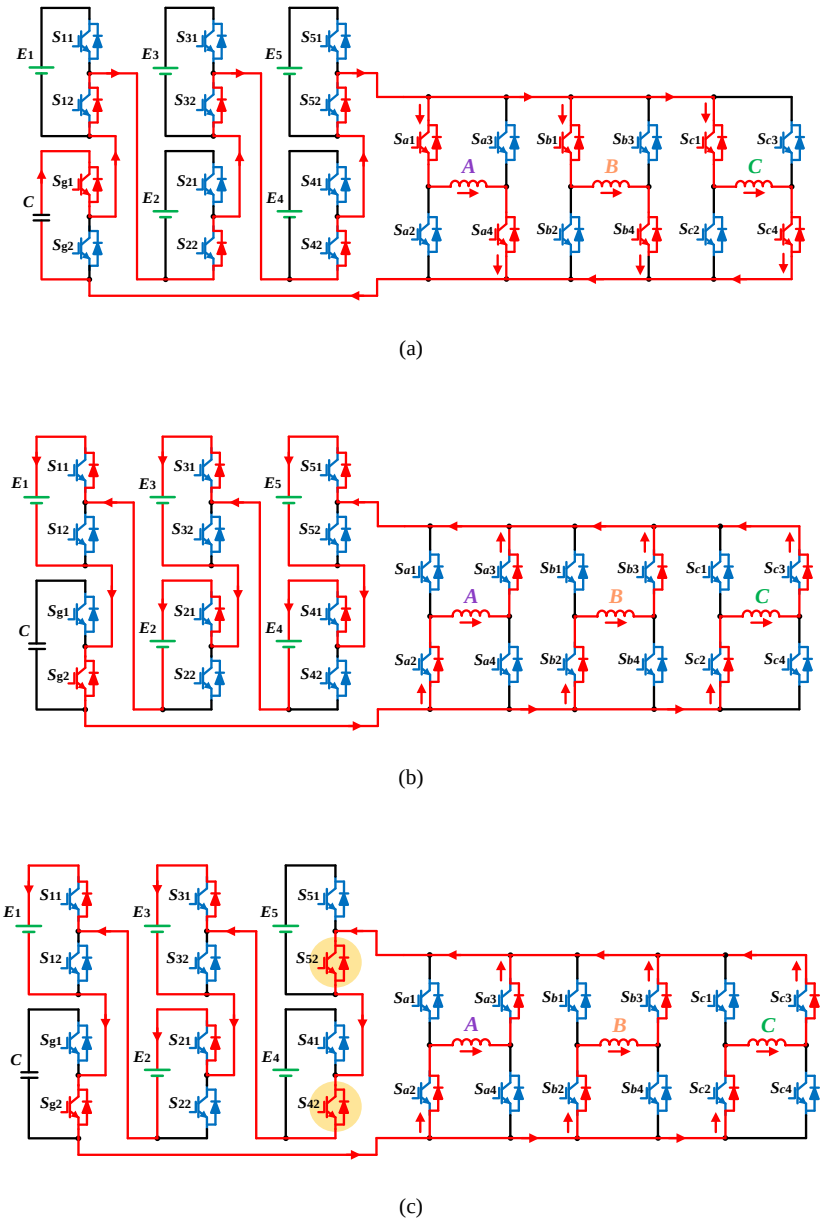

Fig. 10. Battery charging under standstill condition. (a) Winding excitation by the rectification from GCU/grids. (b) E_1~E_5 charging from GCU/grids. (c) E_1, E_2 and E_3 charging from GCU/grids.

There are two operation modes for the battery charging, including the phase current continuous mode and phase current discontinuous mode, which are determined by the duty-cycle and switching frequency of driving signals for the full-bridge converter. In the phase current continuous mode, the discharging and charging currents by employing one phase can be expressed according to different stages as

$$i_{kby}(t)=\begin{cases} I_{k0}+\dfrac{I_{km}-I_{k0}}{DT_s}t, & 0\le t\le DT_s \\ I_{km}-\dfrac{I_{km}-I_{k0}}{(1-D)T_s}(t-DT_s), & DT_s<t\le T_s \end{cases} \tag{18}$$

where I_{k0} is the initial phase current, I_{km} is the maximum phase current, and D and T_s are the switching period and duty cycle of the PWM signal, respectively.

When three phase windings are all used for charging, the sum of the maximum and minimum currents flowing through the phase windings are given by

$$\begin{cases} I_{\max} = I_{am} + I_{bm} + I_{cm} \\ I_{\min} = I_{a0} + I_{b0} + I_{c0} \end{cases} \tag{19}$$

Hence, the discharging and charging currents with three phases are expressed as

$$i_{by}(t) = \begin{cases} I_{\min} + \dfrac{I_{\max} - I_{\min}}{DT_s} t, & 0 \le t \le DT_s \\ I_{\max} - \dfrac{I_{\max} - I_{\min}}{(1-D)T_s}(t - DT_s), & DT_s < t \le T_s \end{cases} \tag{20}$$

In the phase current discontinuous mode, considering the discontinuous current, the discharging and charging currents are expressed as

$$i_{by}(t) = \begin{cases} I_{\min} + \dfrac{I_{\max} - I_{\min}}{DT_s} t, & 0 \le t \le DT_s \\ I_{\max} - \dfrac{I_{\max} - I_{\min}}{(1-D)T_s}(t - DT), & DT_s < t \le T_0 \\ 0, & T_0 < t \le T_s \end{cases} \tag{21}$$

where T_0 is the charging current ending period.

F. Battery Fault-Tolerance Mode

A battery system may consist of many battery cells, and each battery cell has a normal operating mode and would also be subject to faults. Serious conditions such as high heat generation, overcharge or over-discharge event, ageing of the battery would result in battery faults and cause irreversible and catastrophic damages during the vehicle running process [51]-[54]. When serious battery faults occur, the HEV will work in unsafety conditions if the faulty ones are still used. However, if the faulty battery cells can be bypassed through control, it will significantly increase the reliability of the whole system. Hence, a fault-tolerance method for the battery system is much important in safety-critical vehicle applications.

The proposed SRM drive can provide flexible fault tolerance control for the battery system. In battery driving mode, if E_5 has a fault, the switch S_{52} can be turned on to bypass E_5, and the current will flow through S_{52} instead of E_5, as shown in Fig. 11(a). Also, the charging current will not go through E_5 due to turning on S_{52}. Hence, the faulty cell E_5 can be easily bypassed by controlling the switch in the corresponding SM. In GCU-battery driving mode, if E_4 and E_5 both have faults, switches S_{42} and S_{52} can be turned

on to bypass E_4 and E_5, and the current will directly go through S_{42} and S_{52}, as shown in Fig. 11(b). Therefore, the battery fault tolerance can be flexibly achieved in both driving and charging conditions under different working modes.

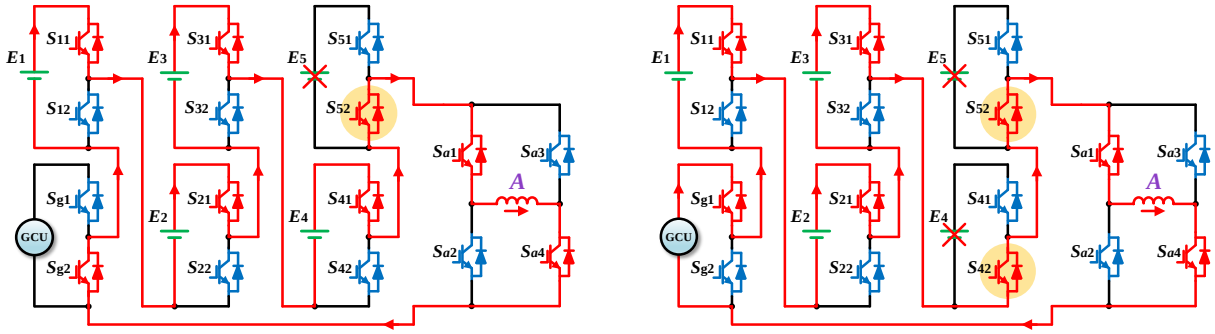

Fig. 11. Battery fault-tolerance control. (a) Battery driving mode with E_5 fault. (b) GCU-battery driving mode with E_4 and E_5 faults.

G. Comparison with Existing Topologies

Fig. 12 presents a qualitative comparison of the proposed MMC-based SRM drive and existing topologies for electric powertrain systems, which shows a superior overall performance. In the figure, the highest score for each item will be obtained if the dc bus voltage can be flexibly controlled at multiple values, a completely modular structure for the converter can be achieved by using commercial power switch modules, each faulty battery pack can be easily bypassed, the battery can be flexibly charged by connecting the grid, each phase is totally isolated and can be independently controlled, and different multilevel voltages can be flexibly achieved and regulated. Otherwise, a lower score will be given.

For the conventional asymmetrical half-bridge converter, the dc bus voltage is fixed and the multilevel voltage cannot be achieved, which limit the torque capability in high-speed operations; the dc bus voltage cannot be changed according to the speed to reduce the voltage stress and switching loss; battery fault tolerance and charging abilities are not equipped; modular structure is not obtained due to the special converter configuration. To achieve the multilevel voltage, four-level converters are proposed in [23], [24]. Although an additional charge capacitor is employed to increase the phase voltage in the excitation and demagnetization regions, the other limitations still exist, which are similar to the asymmetrical converter. To achieve battery charging, modified C-dump converters are presented in [27], [28]. However, the fault-tolerance ability is poor because three phases are not isolated in the circuit, and flexible dc bus voltage and modular structure cannot be achieved. In [29], [30], multiport converters are presented to achieve battery charging, multilevel voltage, and flexible driving control. However, flexible dc bus voltage, fault tolerance for battery cells, and completely modular structure are not achieved. In order to obtain a flexible dc bus voltage and battery charging

ability, a dc-dc converter is employed in the front end of SRM drives [35], [36]. However, additional inductors and capacitors are required, and multilevel voltage, modular structure, and battery fault-tolerance ability are not achieved.

Compared to existing topologies, the MMC is employed for the SRM drive in this paper, where the battery cells are decentralized by the SMs. Standard half-bridge modules are used for both the MMC and full-bridge converter in the proposed motor drive, and thus has a good fault-tolerance ability due to phase isolation and achieves a completely modular structure. Multiple modes/functions can be flexibly achieved by controlling the MMC-based drive, including the battery driving mode, GCU driving mode, GCU-battery driving mode, running charging mode, standstill charging mode, and battery fault-tolerance mode. By using the MMC, flexible dc bus voltage is achieved, which can reduce the voltage stress and switching loss on the switches according to the running speed. The reliability of the motor drive can also be improved due to a lower voltage stress. Multilevel phase voltage is obtained in GCU driving mode, battery driving mode, and hybrid source driving mode, where the torque capability can be improved accordingly. Also, flexible fault-tolerance ability for battery cells is equipped by controlling the switches in corresponding SMs. Furthermore, the battery can be charged in both running and standstill conditions by utilizing the proposed converter without external ones. Battery SOC balance can be easily achieved by selecting the charged battery cells according to the SOC level.

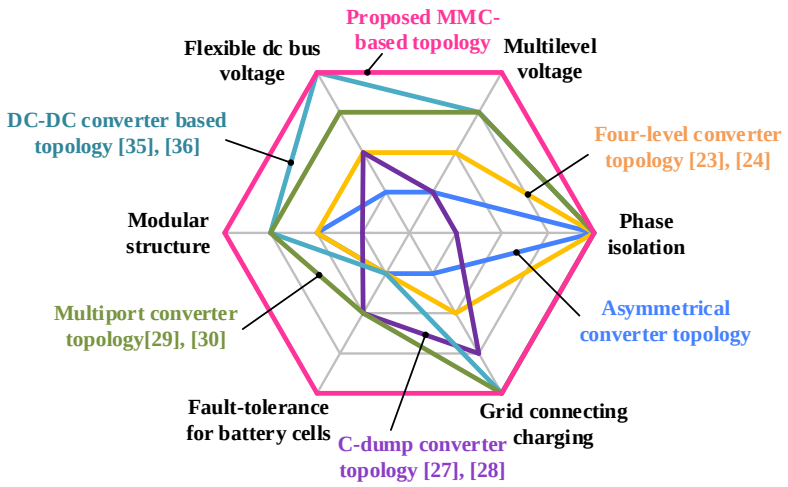

Fig. 12. Qualitative comparison of proposed and existing SRM drive topologies.

IV. Experimental Verification

To verify the effectiveness of the proposed MMC-based SRM drive, experiments are carried out on a scale-down three-phase 12/8 SRM prototype by employing six SMs for proof-of-concept. Table II gives the main parameters of the SRM. The experimental setup is shown in Fig. 13, including the controller, power electronics, and motor test bed. The control algorithm is implemented in a dSPACE-DS1006 platform. The phase currents are detected by Hall-effect current sensors LA-55P for current regulation control.

A proportional integral (PI) controller is employed to implement the closed-loop speed control and the current hysteresis control method is used for phase current regulation. A multi-channel isolated oscilloscope is employed to observe the voltage and current waveforms. In the motor test bed, a Parker AC servomotor is used as the load, which can be controlled by a load controller inside the cabinet. A three-degree-of-freedom (3-DOF) bracket can be adjusted to ensure a balanced connection between the SRM and load motor. A high-precision torque sensor (Lorenz 0261Due) is used to detect the instantaneous output torque. A 2500-line incremental encoder (ZZU4809) is installed on the motor bearing to detect the rotor position and calculate the rotational speed. A programmable dc power source is utilized to simulate the GCU part, where the output voltage is set to 80 V. Five 24V battery packs are employed for the MMC configuration.

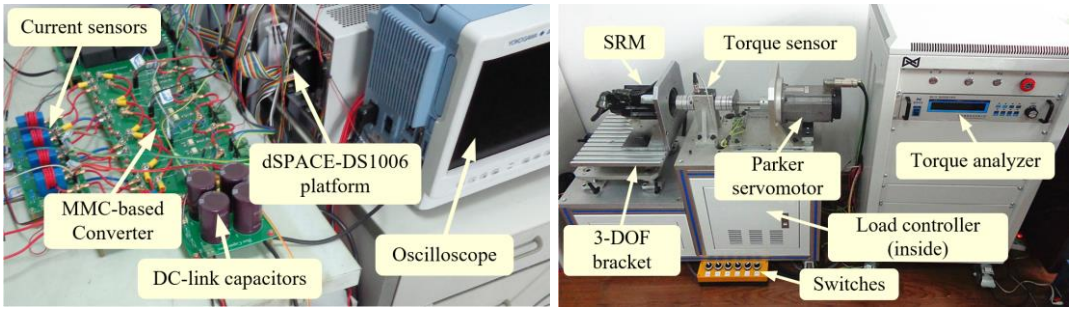

Fig. 13. Experimental setup.

TABLE II

MOTOR PARAMETERS

Parameters	Value
Phase number	3
Stator/rotor poles	12/8
Rated power (W)	750
Rated speed (r/min)	1500
Phase resistor (Ω)	3.01
Minimum phase inductance (mH)	27.2
Maximum phase inductance (mH)	256.7
Rotor outer diameter (mm)	55
Rotor inner diameter (mm)	30
Stator outer diameter (mm)	102.5
Stator inner diameter (mm)	55.5
Stack length (mm)	80
Stator arc angle (deg)	14
Rotor arc angle (deg)	16

Fig. 14 shows the experimental waveforms in battery driving mode at low speed of 300 r/min and 2 N·m load, where i_a, i_b, and i_c are the currents of phase A, phase B, and phase C, respectively, U_a is the phase A voltage, i_{by} is the battery current flowing through full cells, and i_{byx} is the battery current flowing through cell x. When all the battery cells are put into use, the excitation and demagnetization voltages on the phase winding are both the full battery voltage, and the battery cells are charged and discharged alternately in each current period, as shown in Fig. 14(a). When parts of the battery cells are employed as a lower

voltage power supply, the motor drive can work under multilevel phase voltage by additional battery charging during the demagnetization process, where running charging is achieved. As shown in Fig. 14(b), E_1 and E_2 are employed to supply the power, and E_3 and E_4 are used for additional charging. The demagnetization voltage of phase A is directly elevated by E_3 and E_4 charging; the excitation voltage of phase A is also increased in phase A and phase C current overlapping region, when the demagnetization current of phase C is larger than the excitation current of phase A. Due to the multilevel voltage, the excitation and demagnetization processes are both accelerated. Battery cells E_3 and E_4 are charged by the demagnetization current of each phase. In Fig. 14(c), E_1 is employed as the power supply, and E_2 and E_5 are used for additional charging, where multilevel phase voltage is also achieved. Therefore, in battery driving mode, the dc bus voltage can be flexibly changed according to the requirement, the voltage stress on the switches can be dramatically reduced, and the battery cells can be flexibly selected for additional charging during the demagnetization process according to the SOC level. Hence, the energy can be transferred among the battery cells to achieve the SOC balance.

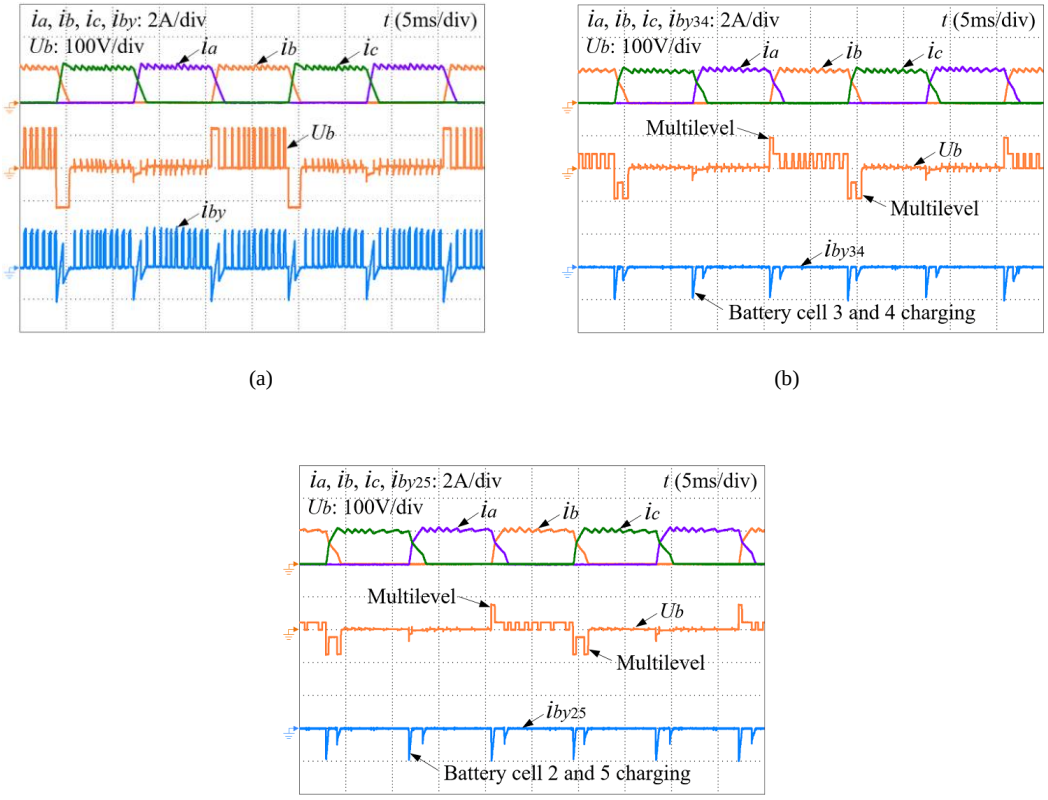

Fig. 14. Battery driving mode at low speed. (a) Driven by full voltage. (b) Driven by E_1 and E_2 with E_3 and E_4 charging. (c) Driven by E_1 with E_2 and E_5 charging.

Fig. 15 illustrates the experimental waveforms in GCU driving mode at 1750 r/min. When the motor is driven by the GCU without additional battery charging, the phase voltage is directly the GCU output voltage both in the excitation and demagnetization

processes, as shown in Fig. 15(a). However, when additional battery charging is employed in the demagnetization process, as shown in Fig. 15(b), multilevel phase voltage is achieved and battery SOC can be balanced by controlling the charging cells. The experimental results in GCU-battery hybrid source driving mode with and without additional battery charging at 2100 r/min and 2250 r/min are presented in Fig. 16(a) and (b), respectively. Similarly, the phase voltage can also be elevated by additional battery charging and the dc bus voltage can be flexibly changed by employing different cells for excitation according to the running speed.

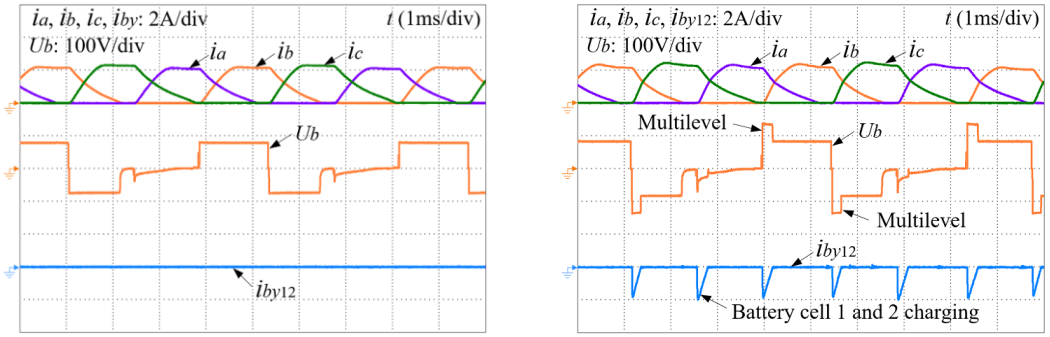

(a) (b)

Fig. 15. GCU driving mode at high speed. (a) Driven by GCU without additional battery charging. (b) Driven by GCU with E_1 and E_2 charging.

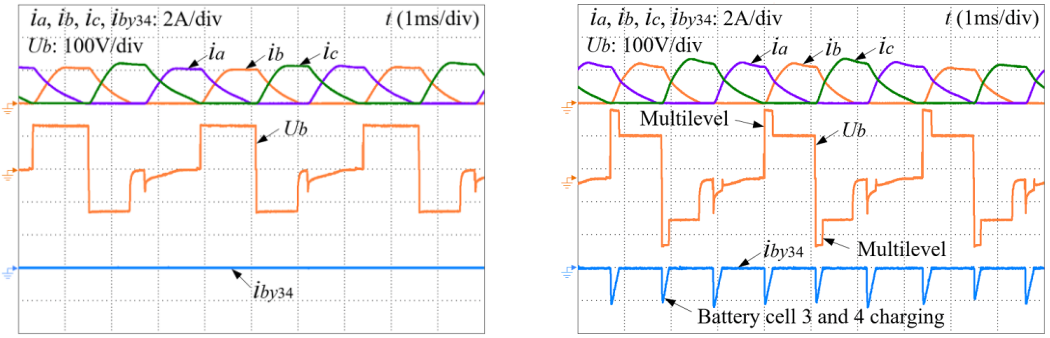

(a) (b)

Fig. 16. GCU-battery driving mode at high speed. (a) Driven by GCU, E_1, and E_2 without additional battery charging. (b) Driven by GCU, E_1, and E_2 with E_3 and E_4 charging.

In standstill conditions, the battery can also be flexibly charged from GCU/grids through the proposed drive, as shown in Fig. 17, where P_Z is the encoder output signal. PWM signals are applied to the switches in the full-bridge converter for the battery charging. In the high level of the PWM, corresponding switches for each phase are turned on, and the capacitor C supplies the power to three phase windings, simultaneously; in the low level of the PWM, the related switches are all turned off, and the energy stored in phase windings feeds back to the power source and charges the battery. Fig. 17 shows the waveforms when the phase current is discontinuous and continuous by employing all battery cells for charging, where the duty cycle is 0.6 and 0.7, respectively.

The encoder output signal stays at zero, and thus the charging scheme does not lead to motor movement. The battery cells can be flexibly selected for charging or bypassed, by controlling the switches in the SMs.

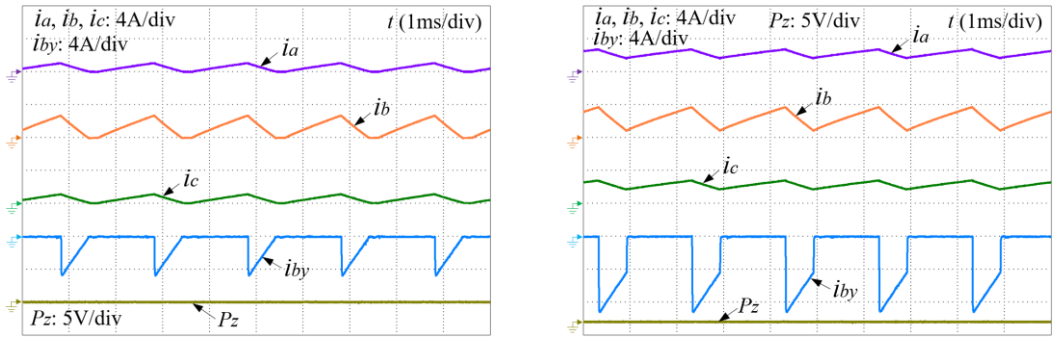

Fig. 17. Standstill battery charging mode. (a) Phase current discontinuous mode. (b) Phase current continuous mode.

In battery fault-tolerance mode, the faulty battery cells can be easily bypassed by controlling the switches in SMs. Fig. 18(a) shows the voltage step in battery driving mode with full cells when E_5 is bypassed, where the bus voltage changes from 120 to 96 V. Fig. 18(b) shows the voltage step in hybrid source driving mode with GCU and E_1~E_4 when E_3 and E_4 are bypassed, where the bus voltage changes from 176 to 128 V. Clearly, there is no obvious fluctuation on the phase currents and speed, and the system can be steadily controlled during the transient process.

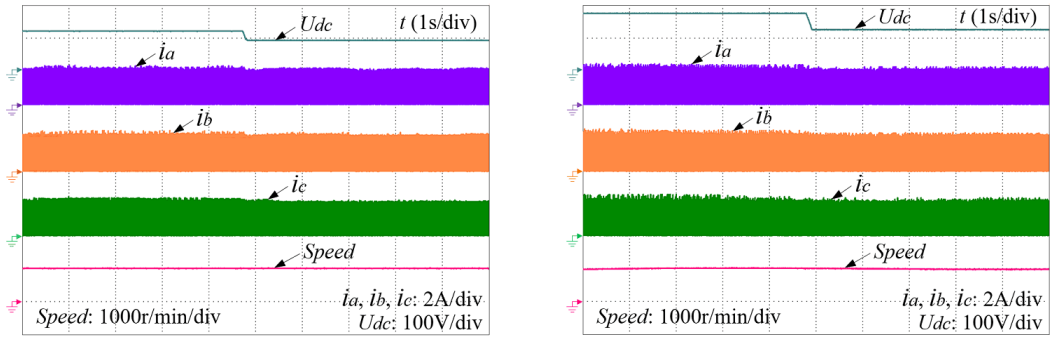

Fig. 18. Battery fault-tolerance mode. (a) Voltage step in battery driving mode with full cells when E_5 is bypassed. (b) Voltage step in GCU-battery driving mode with GCU and E_1~E_4 when E_3 and E_4 are bypassed.

In order to investigate the dynamic performance of the proposed SRM drive, Fig. 19 shows the experimental waveforms under the speed step change, load step change, and braking conditions. As shown in Fig. 19(a), when the speed reference changes from 300 to 800 r/min and 800 to 1200 r/min with a 2 N·m load, the instantaneous speed quickly tracks the given reference and follows

the reference well. When a load step from 2 to 4 N·m is applied, the instantaneous speed is still stabilized in a very short time, as shown in Fig. 19(b). In the braking process, the battery can be directly charged by the braking current, where the turn-on and turn-off angles can be adjusted to achieve flexible braking performance. When the turn-on and turn-off angles are set to 20 °and 30 °, respectively, the braking process is finished in 2 s; while when the turn-off angle is extended to 40 °, the braking process can be controlled within 1s. It can be seen from the experimental results that the proposed drive has a good dynamic performance to transient changes.

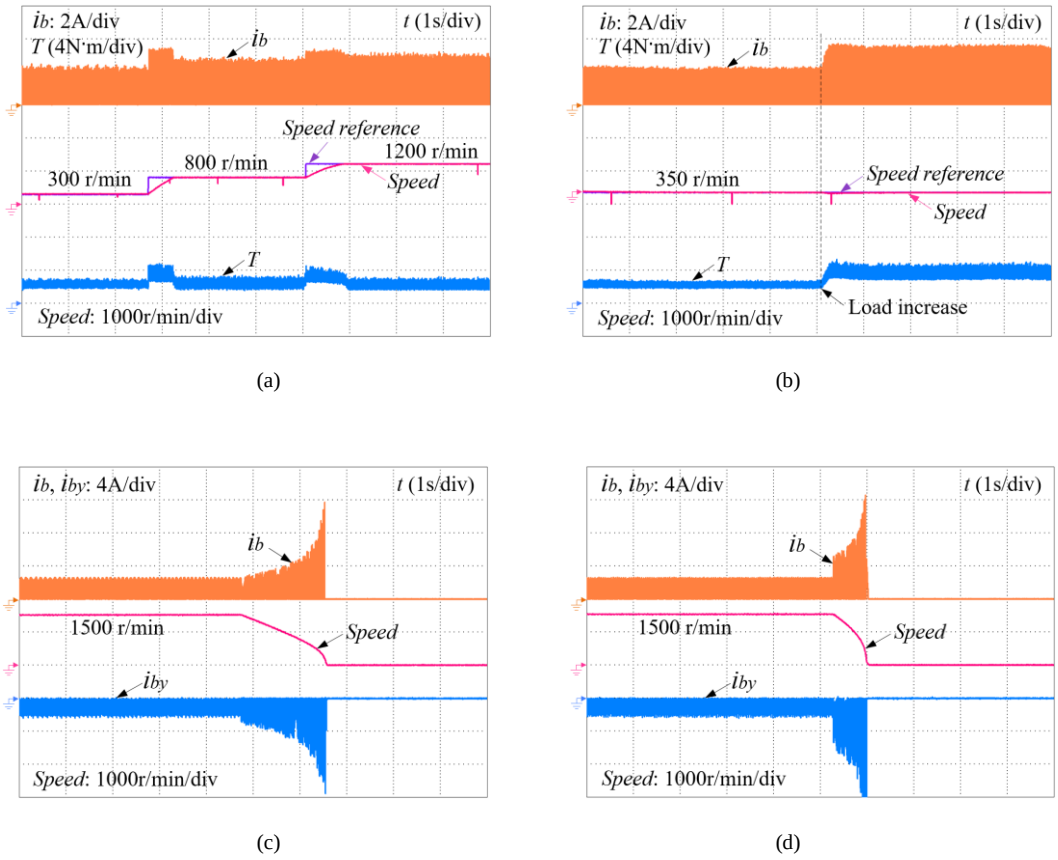

Fig. 19. Dynamic performance. (a) Speed step change. (b) Load step change. (c) Braking with turn-on angle 20 °and turn-off angle 30 °. (d) Braking with turn-on angle 20 °and turn-off angle 40 °.

Fig. 20 presents the torque comparison between the proposed MMC-based SRM drive with multilevel phase voltage and conventional drive without multilevel phase voltage in battery driving mode and GCU driving mode, respectively. Fig. 20(a) shows the condition that battery cell E_1 and E_2 are used to supply the power to the motor, and E_3 and E_4 are additionally employed in the demagnetization mode for multilevel voltage. Fig. 20(b) shows the condition that the GCU is used as the power source and E_1~E_4 are employed for multilevel voltage. By employing additional battery charging in the phase demagnetization mode, multilevel

phase voltage can be flexibly achieved, where the winding excitation and demagnetization processed are both accelerated. The torque can be improved by 28% due to the multilevel voltage, especially in high-speed operations.

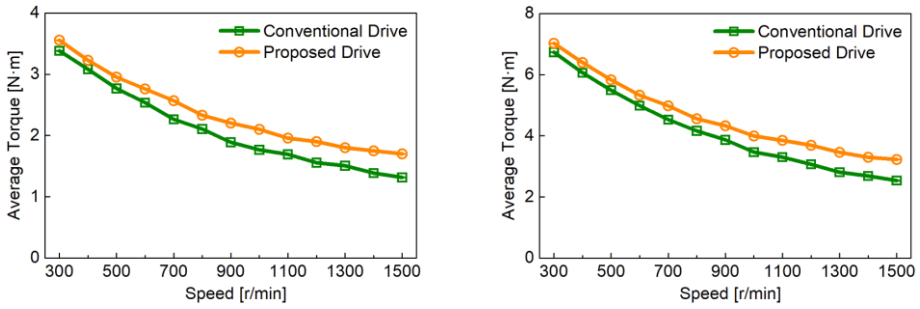

(a) (b)

Fig. 20. Torque comparison. (a) Battery driving mode. (b) GCU driving mode.

Fig. 21 shows the system efficiency comparison between the proposed and conventional drives with and without the multilevel voltage and variable dc bus voltage. Fig. 21(a) gives the efficiency comparison in battery driving mode with 2 N·m load and Fig. 21(b) presents the efficiency comparison in GCU-battery driving mode with 4 N·m load. For the conventional drive, all the battery cells are employed to supply the power in both battery driving mode and hybrid source driving mode, where the multilevel voltage and variable dc bus voltage are not achieved. In order to improve the system performance, multilevel phase voltage is achieved and the dc bus voltage is also adjusted to a lower value according to the running speed. From the comparison, it can be seen that the system efficiency can be improved by 2% in the proposed drive due to both the multilevel voltage and variable dc bus voltage.

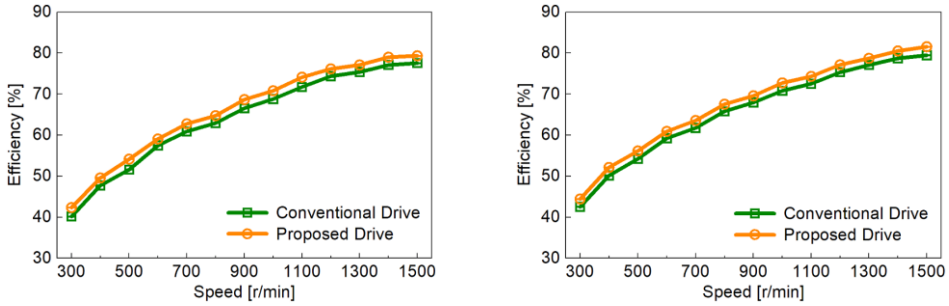

(a) (b)

Fig. 21. Efficiency comparison. (a) Battery driving mode. (b) GCU-battery driving mode.

It should be noted that, in order to explain the functions and operation modes of the proposed SRM drive more clearly, only six SMs are adopted in this paper for analysis and experiments. However, more flexible dc bus voltage, battery charging, multilevel phase voltage, and battery fault tolerance ability can be further achieved by employing more SMs for the proposed motor system.

V. Conclusion

In this paper, a MMC-based SRM drive is proposed for HEV applications, which not only improves the motor system performance with variable dc bus voltage and multilevel voltage, but also achieves flexible charging functions and battery fault-tolerance ability. In the proposed drive, the MMC is employed for the BESS, where battery cells are decentralized by SMs. In order to achieve a modular structure, the full-bridge converter is used to drive the motor. Multiple modes/functions can be achieved by controlling the SMs in the MMC, including the battery driving mode, GCU driving mode, GCU-battery driving mode, running charging mode, standstill charging mode, and battery fault-tolerance ability. The main contributions and advantages of this paper are as follows:

1) Flexible dc bus voltage is achieved by selecting the working SMs according to the running speed, which can reduce the voltage stress on the switches and also improve the system reliability.

2) Multilevel phase voltage is obtained by employing additional battery cell charging in the demagnetization process, where the torque capability can be improved accordingly.

3) Modular structure is achieved by using standard half-bridge modules, which is beneficial for the market mass production.

4) Flexible charging functions are achieved, including the running charging and standstill charging. The battery can be directly charged by the demagnetization current during the running condition or braking process. In standstill conditions, the battery can also be charged from the GCU or grids through the proposed drive without external ones.

5) Flexible fault-tolerance ability for battery cells is achieved by controlling the switch in corresponding SM.

6) Battery SOC balance can be easily achieved by selecting the charged battery cells according to the SOC level, no matter in running or standstill charging conditions.

Although this work has targeted electrified vehicle applications, the developed technology can also be applied to other applications, such as more-electric aircraft, traction drives, and electrical ships.

References

[1] S. S. Williamson, A. K. Rathore, and F. Musavi, “Industrial electronics for electric transportation: current state-of-the-art and future challenges,” *IEEE Trans. Ind. Electron.* vol. 62, no. 5, pp. 3021-3032, May 2015.

[2] A. A. Ferreira, J. A. Pomilio, G. Spiazzi, and L. de Araujo Silva, “Energy management fuzzy logic supervisory for electric vehicle power supplies system,” *IEEE Trans. Power Electron.*, vol. 23, no. 1, pp. 107-115, Jan. 2008.

[3] G. Carli and S. S. Williamson, “Technical considerations on power conversion for electric and plug-in hybrid electric vehicle battery charging in photovoltaic installations,” *IEEE Trans. Power Electron.*, vol. 28, no. 12, pp. 5784-5792, Dec. 2013.

[4] O. C. Onar, J. Kobayashi, and A. Khaligh, “A fully directional universal power electronic interface for EV, HEV, and PHEV applications,” *IEEE Trans. Power Electron.*, vol. 28, no. 12, pp. 5489-5498, Dec. 2013.

[5] A. Emadi, Y. J. Lee, and K. Rajashekara, "Power electronics and motor drives in electric, hybrid electric, and plug-in hybrid electric vehicles," *IEEE Trans. Ind. Electron.*, vol. 55, no. 6, pp. 2237–2245, Jun. 2008.

[6] Z. Yang, F. Shang, I. P. Brown, and M. Krishnamurthy, "Comparative study of interior permanent magnet, induction, and switched reluctance motor drives for EV and HEV applications," *IEEE Trans. Transport. Electrific.*, vol. 1, no. 3, pp. 245-254, Oct. 2015.

[7] I. Boldea, L. N. Tutelea, L. Parsa, and D. Dorrell, "Automotive electric propulsion systems with reduced or no permanent magnets: an overview," *IEEE Trans. Ind. Electron.*, vol. 61, no. 10, pp. 5696-5711, Oct. 2014.

[8] M. Krishnamurthy, C. S. Edrington, A. Emadi, P. Asadi, M. Ehsani, and B. Fahimi, "Making the case for applications of switched reluctance motor technology in automotive products," *IEEE Trans. Power Electron.*, vol. 21, no. 3, pp. 659-675, May 2006.

[9] E. Bostanci, M. Moallem, A. Parsapour, and B. Fahimi, "Opportunities and challenges of switched reluctance motor drives for electric propulsion: a comparative study," *IEEE Trans. Transport. Electrific.*, vol. 3, no. 1, pp. 58-75, Mar. 2017.

[10] J. Cai and Z. Deng, "Unbalanced phase inductance adaptable rotor position sensorless scheme for switched reluctance motor," *IEEE Trans. Power Electron.*, vol. PP, no. 99, pp. 1-8. (in press)

[11] A. Chiba, K. Kiyota, N. Hoshi, M. Takemoto, and S. Ogasawara, "Development of a rare-earth-free SR motor with high torque density for hybrid vehicles," *IEEE Trans. Energy Convers.*, vol. 30, no. 1, pp. 175-182, Mar. 2015.

[12] B. Bilgin, A. Emadi, and M. Krishnamurthy, "Comprehensive evaluation of the dynamic performance of a 6/10 SRM for traction application in PHEVs," *IEEE Trans. Ind. Electron.*, vol. 60, no. 7, pp. 2564-2575, Jul. 2013.

[13] J. Ye, B. Bilgin, and A. Emadi, "An extended-speed low-ripple torque control of switched reluctance motor drives," *IEEE Trans. Power Electron.*, vol. 30, no. 3, pp. 1457-1470, Mar. 2015.

[14] W. Ding, S. Yang, Y. Hu, S. Li, T. Wang and Z. Yin, "Design consideration and evaluation of a 12/8 high-torque modular-stator hybrid excitation switched reluctance machine for EV applications," *IEEE Trans. Ind. Electron.*, vol. 64, no. 12, pp. 9221-9232, Dec. 2017.

[15] H. Chen and J. J. Gu, "Implementation of the three-phase switched reluctance machine system for motors and generators," *IEEE/ASME Trans. Mechatronics*, vol. 15, no. 3, pp. 421–432, Jun. 2010.

[16] M. A. Kabir, and I. Husain, "Design of mutually coupled switched reluctance motors (MCSRMs) for extended speed applications using 3-phase standard inverters," *IEEE Trans. Energy Convers.*, vol. 31, no. 2, pp. 436-445, Jun. 2016.

[17] R. Martin, J. D. Widmer, B. C. Mecrow, M. Kimiabeigi, A. Mebarki, and N. L. Brown, "Electromagnetic considerations for a six-phase switched reluctance motor driven by a three-phase inverter," *IEEE Trans. Ind. Appl.*, vol. 52, no. 5, pp. 3783-3791, Sep./Oct. 2016.

[18] S. Song, Z. Xia, Z. Zhang, and W. Liu, "Control performance analysis and improvement of a modular power converter for three-phase SRM with Y-connected windings and neutral line," *IEEE Trans. Ind. Electron.*, vol. 63, no. 10, pp. 6020-6030, Oct. 2016.

[19] S. Song, Z. Xia, G. Fang, R. Ma and W. Liu, "Phase current reconstruction and control of 3-phase switched reluctance machine with modular power converter using single dc-link current sensor," *IEEE Trans. Power Electron.*, vol. PP, no. 99, pp. 1-1. (in press)

[20] F. Peng, J. Ye and A. Emadi, "An asymmetric three-level neutral point diode clamped converter for switched reluctance motor drives," *IEEE Trans. Power Electron.*, vol. 32, no. 11, pp. 8618-8631, Nov. 2017.

[21] A. K. Mishra and B. Singh, "Solar photovoltaic array dependent dual output converter based water pumping using switched reluctance motor drive," *IEEE Trans. Ind. Appl.*, vol. 53, no. 6, pp. 5615-5623, Nov.-Dec. 2017.

[22] F. Yi, and W. Cai, "A quasi-Z-source integrated multiport power converter as switched reluctance motor drives for capacitance reduction and wide-speed-range operation," *IEEE Trans. Power Electron.*, vol. 31, no. 11, pp. 7661-7676, Nov. 2016.

[23] D. H. Lee, and J. W. Ahn, "A novel four-level converter and instantaneous switching angle detector for high speed SRM drive," *IEEE Trans. Power Electron.*, vol. 22, no. 5, pp. 2034-2041, Sep. 2007.

[24] J. Liang, D. H. Lee, G. Xu, and J. W. Ahn, "Analysis of passive boost power converter for three-phase SR drive," *IEEE Trans. Ind. Electron.*, vol. 57, no. 9, pp. 2961-2971, Sep. 2010.

[25] A. K. Jain, and N. Mohan, "SRM power converter for operation with high demagnetization voltage," *IEEE Trans. Ind. Appl.*, vol. 41, no. 5, pp. 1224-1231, Sep./Oct. 2005.

[26] Y. Hu, C. Gan, W. Cao, C. Li, and S. J. Finney, "Split converter-fed SRM drive for flexible charging in EV/HEV applications," *IEEE Trans. Ind. Electron.*, vol. 62, no. 10, pp. 6085-6095, Oct. 2015.

[27] Y. Hu, X. Song, W. Cao, and B. Ji, "New SR drive with integrated charging capacity for plug-in hybrid electric vehicles (PHEVs)," *IEEE Trans. Ind. Electron.*, vol. 61, no. 10, pp. 5722-5731, Oct. 2014.

[28] Y. Hu, C. Gan, W. Cao, Y. Fang, S. J. Finney, and J. Wu, "Solar PV-powered SRM drive for EVs with flexible energy control functions," *IEEE Trans. Ind. Appl.*, vol. 52, no. 4, pp. 3357-3366, Jul./Aug. 2016.

[29] C. Gan, J. Wu, Y. Hu, S. Yang, W. Cao, and J. M. Guerrero, "New integrated multilevel converter for switched reluctance motor drives in plug-in hybrid electric vehicles with flexible energy conversion," *IEEE Trans. Power Electron.*, vol. 32, no. 5, pp. 3754-3766, May 2017.

[30] C. Gan, N. Jin, Q. Sun, W. Kong, Y. Hu, and L. M. Tolbert, "Multiport bidirectional SRM drives for solar-assisted hybrid electric bus powertrain with flexible driving and self-charging functions," *IEEE Trans. Power Electron.*, vol. PP, no. 99, pp. 1-1. (in press)

[31] H. C. Chang and C. M. Liaw, "An integrated driving/charging switched reluctance motor drive using three-phase power module," *IEEE Trans. Ind. Electron.*, vol. 58, no. 5, pp. 1763-1775, May 2011.

[32] C. Y. Yu, J. Tamura, and R. D. Lorenz, "Optimum dc bus voltage analysis and calculation method for inverters/motors with variable dc bus voltage," *IEEE Trans. Ind. Appl.*, vol. 49, no. 6, pp. 2619-2627, Nov./Dec. 2013.

[33] M. Amiri, H. Farzanehfard and E. Adib, "A nonisolated ultrahigh step down dc–dc converter with low voltage stress," *IEEE Trans. Ind. Electron.*, vol. 65, no. 2, pp. 1273-1280, Feb. 2018.

[34] D. Panda, and V. Ramanarayanan, "Reduced acoustic noise variable dc-bus-voltage-based sensorless switched reluctance motor drive for HVAC applications," *IEEE Trans. Ind. Electron.*, vol. 54, no. 4, pp. 2065-2078, Aug. 2007.

[35] H. C. Chang and C. M. Liaw, "On the front-end converter and its control for a battery powered switched-reluctance motor drive," *IEEE Trans. Power Electron.*, vol. 23, no. 4, pp. 2143-2156, Jul. 2008.

[36] K. Hu, P. Yi, and C. Liaw, "An EV SRM drive powered by battery/supercapacitor with G2V and V2H/V2G capabilities," *IEEE Trans. Ind. Electron.*, vol. 62, no. 8, pp. 4714-4727, Aug. 2015.

[37] Y. S. Kumar and G. Poddar, "Control of medium-voltage AC motor drive for wide speed range using modular multilevel converter," *IEEE Trans. Ind. Electron.*, vol. 64, no. 4, pp. 2742-2749, Apr. 2017.

[38] B. Tai, C. Gao, X. Liu and Z. Chen, "A novel flexible capacitor voltage control strategy for variable-speed drives with modular multilevel converters," *IEEE Trans. Power Electron.*, vol. 32, no. 1, pp. 128-141, Jan. 2017.

[39] M. Quraan, P. Tricoli, S. D'Arco and L. Piegari, "Efficiency assessment of modular multilevel converters for battery electric vehicles," *IEEE Trans. Power Electron.*, vol. 32, no. 3, pp. 2041-2051, Mar. 2017.

[40] Y. Okazaki, W. Kawamura, M. Hagiwara, H. Akagi, T. Ishida, M/ Tsukakoshi, and R. Nakamura, "Experimental comparisons between modular multilevel DSCC inverters and TSBC converters for medium-voltage motor drives," *IEEE Trans. Power Electron.*, vol. 32, no. 3, pp. 1805-1817, Mar. 2017.

[41] D. Patil, S. Wang, and L. Gu, "Multilevel converter topologies for high-power high-speed switched reluctance motor: performance comparison," *IEEE Applied Power Electronics Conference and Exposition*, Long Beach, CA, pp. 2889-2896, 2016.

[42] Q. Chen, D. Xu, L. Xu, J. Wang, Z. Lin, and X. Zhu, "Fault-tolerant operation of a novel dual-channel switched reluctance motor using two 3-phase standard inverters," *IEEE Trans. Appl. Supercond.*, vol. 28, no. 3, pp. 1-5, Apr. 2018.

[43] K. Tungpimolrut, S. Kachapornkul, P. Jitkreeyarn, P. Somsiri, N. Chayopitak, and C. Akira, "Bipolar excitation for double three-phase full bridge converter based three-phase switched reluctance motor drive system," *Annual Conference of the IEEE Industrial Electronics Society*, Vienna, pp. 2626-2631, 2013.

[44] H. C. Chang, C. H. Chen, Y. H. Chiang, W. Y. Sean and C. M. Liaw, "Establishment and control of a three-phase switched reluctance motor drive using intelligent power modules," *IET Elect. Power Appl.*, vol. 4, no. 9, pp. 772-782, Nov. 2010.

[45] S. Chung and O. Trescases, "Hybrid energy storage system with active power-mix control in a dual-chemistry battery pack for light electric vehicles," *IEEE Trans. Transp. Electrific.*, vol. 3, no. 3, pp. 600-617, Sep. 2017.

[46] C. Duan, C. Wang, Z. Li, J. Chen, S. Wang, A. Snyder, and C. Jiang, "A solar power assisted battery balancing system for electric vehicles," *IEEE Trans. Transp. Electrific.*, vol. PP, no. 99, pp. 1-11, 2018. (in press)

[47] J. I. Y. Ota, T. Sato, and H. Akagi, "Enhancement of performance, availability, and flexibility of a battery energy storage system based on a modular multilevel cascaded converter (MMCC-SSBC)," *IEEE Trans. Power Electron.*, vol. 31, no. 4, pp. 2791-2799, Apr. 2016.

[48] N. Kawakami, S. Ota, H. Kon, S. Konno, H. Akagi, H. Kobayashi, and N. Okada, "Development of a 500-kW modular multilevel cascade converter for battery energy storage systems," *IEEE Trans. Ind. Appl.*, vol. 50, no. 6, pp. 3902-3910, Nov./Dec. 2014.

[49] Z. Zheng, K. Wang, L. Xu and Y. Li, "A hybrid cascaded multilevel converter for battery energy management applied in electric vehicles," *IEEE Trans. Power Electron.*, vol. 29, no. 7, pp. 3537-3546, Jul. 2014.

[50] J. Dixon, J. Pereda, C. Castillo and S. Bosch, "Asymmetrical multilevel inverter for traction drives using only one DC supply," *IEEE Trans. Veh. Technol.*, vol. 59, no. 8, pp. 3736-3743, Oct. 2010.

[51] L. Maharjan, T. Yamagishi, H. Akagi and J. Asakura, "Fault-tolerant operation of a battery-energy-storage system based on a multilevel cascade PWM converter with star configuration," *IEEE Trans. Power Electron.*, vol. 25, no. 9, pp. 2386-2396, Sep. 2010.

[52] A. Sidhu, A. Izadian and S. Anwar, "Adaptive nonlinear model-based fault diagnosis of Li-Ion batteries," *IEEE Trans. Ind. Electron.*, vol. 62, no. 2, pp. 1002-1011, Feb. 2015.

[53] A. C. Arenas, S. Onori, and G. Rizzoni, "A control-oriented lithium-ion battery pack model for plug-in hybrid electric vehicle cycle-life studies and system design with consideration of health management", *Journal of Power Sources*, vol. 279, no. 1, pp. 791-808, Apr. 2015

[54] Z. Yang, D. Patil, and B. Fahimi, "Online estimation of capacity fade and power fade of lithium-ion batteries based on input–output response technique," *IEEE Trans. Transport. Electrific.*, vol. 4, no. 1, pp. 147-156, Mar. 2018.